Organic & Biomolecular Chemistry

Selective Binding of Anions by Rigidified Nanojars: Sulfate vs. Carbonate

Journal:	*Organic & Biomolecular Chemistry*
Manuscript ID	OB-ART-07-2021-001318.R1
Article Type:	Paper
Date Submitted by the Author:	04-Aug-2021
Complete List of Authors:	Al Isawi, Wisam ; Western Michigan University, Chemistry Salome, Austin; Western Michigan University, Chemistry Ahmed, Basil; Western Michigan University, Chemistry Zeller, Matthias; Purdue University, Department of Chemistry Mezei, Gellert; Western Michigan University, Chemistry

Selective Binding of Anions by Rigidified Nanojars: Sulfate vs. Carbonate

Wisam A. Al Isawi,[a†] Austin Z. Salome,[a†] Basil M. Ahmed,[a] Matthias Zeller[b] and Gellert Mezei[a*]

[a] *Department of Chemistry, Western Michigan University, Kalamazoo, Michigan 49008, USA*

[b] *Department of Chemistry, Purdue University, West Lafayette, Indiana 47907, USA*

†These authors contributed equally to this work

*Corresponding author. Email: gellert.mezei@wmich.edu

Abstract

Selective binding and transport of highly hydrophilic anions is ubiquitous in nature, as anion binding proteins can differentiate between similar anions with over a million-fold efficiency. While comparable selectivity has occasionally been achieved for certain anions using small, artificial receptors, the selective binding of certain anions, such as sulfate in the presence of carbonate, remains a very challenging task. Nanojars of the formula $[anion\subset\{Cu(OH)(pz)\}_n]^{2-}$ (pz = pyrazolate; n = 27–33) are totally selective for either CO_3^{2-} or SO_4^{2-} over anions such as NO_3^-, ClO_4^-, BF_4^-, Cl^-, Br^- and I^-, but cannot differentiate between the two. We hypothesized that rigidification of the nanojar outer shell by tethering pairs of pyrazole moieties together will restrict the possible orientations of the OH hydrogen-bond donor groups in the anion-binding cavity of nanojars, similarly to anion-binding proteins, and will lead to selectivity. Indeed, by using either homoleptic or heteroleptic nanojars of the general formula $[anion\subset Cu_n(OH)_n(\mathbf{L2}–\mathbf{L6})_y(pz)_{n-2y}]^{2-}$ (n = 26–31) based on a series of homologous ligands $HpzCH_2(CH_2)_xCH_2pzH$ (x = 0–4; $H_2\mathbf{L2}$–$H_2\mathbf{L6}$), selectivity for carbonate (with **L2** and with **L4**–**L6**/pz mixtures) or for sulfate (with **L3**) has been achieved. The synthesis of new ligands $H_2\mathbf{L3}$, $H_2\mathbf{L4}$ and $H_2\mathbf{L5}$, X-ray crystal structures of $H_2\mathbf{L4}$ and the tetrahydropyranyl-protected derivatives $(THP)_2\mathbf{L4}$ and $(THP)_2\mathbf{L5}$, synthesis and characterization by electrospray-ionization mass spectrometry (ESI-MS) of carbonate- and sulfate-nanojars derived from ligands $H_2\mathbf{L2}$–$H_2\mathbf{L6}$, as well as detailed selectivity studies for CO_3^{2-} vs. SO_4^{2-} using these novel nanojars are presented.

1. Introduction

Selective recognition, binding and transport of small inorganic anions by molecular receptors are essential features of a number of natural and industrial processes, such as anion transport in biological systems[1] and removal of harmful anions from contaminated aqueous environments.[2] Natural anion-binding proteins are able to bind specific inorganic anions with high affinity and selectivity, by using a multitude of hydrogen bonds to wrap around the anion and totally isolating it from its surrounding medium. For example, the sulfate-binding protein (SBP) of *Salmonella typhimurium* binds sulfate (K_a = 8.3 × 10^6 for SO_4^{2-}) five orders of magnitude stronger than phosphate ($K_a \simeq 17$ for HPO_4^{2-}).[3] Similarly, the phosphate-binding protein (PBP) of *Pseudomonas fluorescens* binds phosphate five orders of magnitude stronger than sulfate.[4] The key to this extraordinary selectivity lies in the protonation state difference of the two otherwise very similar anions (S–O: 1.49 Å; P–O: 1.52/1.59 Å). At neutral pH, such as in the cytosol, sulfate exists exclusively as SO_4^{2-}, while phosphate exists as a 62/38 mixture of $H_2PO_4^-$ and HPO_4^{2-}. Crystallographic studies have shown that the anion binding site of the SBP lacks hydrogen bond acceptors, therefore SBP binds only fully ionized, tetrahedral oxyacid dianions. The difference in binding affinity of SBP for sulfate versus similar dianions, such as chromate (Cr–O: 1.60 Å) and selenate (Se–O: 1.65 Å), however, is poor: K_a = 3.3 × 10^6 for CrO_4^{2-} and K_a = 2.0 × 10^5 for SeO_4^{2-}.[3] Yet, the PBP of *Pseudomonas fluorescens* is able to bind HPO_4^{2-} with a 4500-fold selectivity over $HAsO_4^{2-}$ (As–O: 1.67/1.73 Å). In this latter case, one single, short H-bond is the key to the selective binding. Although the effect of the difference in the P–O and As–O bond lengths on the twelve donor–acceptor H-bond distances and the overall protein structure is negligible, the slightly longer As–O bond places the H-atom in a less favorable position for hydrogen bonding in the case of $HAsO_4^{2-}$ (∢PO–H···O = 179.1(5)°; ∢AsO–H···O = 163(2)°).[4] The crucial role of the short H-bond in selectivity is further demonstrated by a different PBP, isolated from *Clostridium perfringens*, which lacks this short H-bond and its selectivity for phosphate over arsenate is diminished to ~150-fold.[5]

It is apparent that anion-binding proteins possess highly sophisticated binding pockets that allow for discrimination between similar anions.[6] Binding studies of sulfate vs. phosphate have shown that charge–charge interactions are not the dominant factor in

binding and emphasize the importance of hydrogen bonding in the recognition and selective binding of anions.[7] The high level of spatial organization of hydrogen bond donors and acceptors in the binding pockets of proteins is made possible by the intricate structure of the protein backbone. Their large size (30–40 kDa), however, renders the industrial-scale use of proteins as anion-binding and extraction agents unfeasible. Therefore, considerable attention is being focused on the binding of anions by small, artificial receptors, as evidenced by the publication of a number of books,[8] book-chapters,[9] themed journal issues[10] and review articles.[11] Several different classes of anion encapsulating agents have been identified, such as macrocycles[12] and cryptands,[11h,13] self-assembled capsules,[11c,14] cyclopeptides,[15] catenanes/rotaxanes,[16] discrete coordination assemblies,[17] metal-organic frameworks[18] and nanoparticles.[19]

The most obvious anion binding agents are positively charged receptors, such as protonated azamacrocycles and cryptands, guanidinium-based hosts, and positively charged coordination complexes and metal-organic frameworks. In these assemblies the anion plays the role of counterion, balancing the positive charge of the host molecule, and is bound predominantly by electrostatic interactions. Specific orientations within the host can be achieved by additional weak interactions, such as hydrogen bonding or interactions with Lewis-acidic metal centers. The disadvantage of protonated organic hosts is that they can only be used under acidic conditions; higher pHs lead to deprotonation and loss of affinity for the anion. Anion binding by neutral receptors was first reported in 1993.[20] Most of the recent examples of neutral anion binding agents are based on tripodal receptors, containing tris(amine),[21] tris(amide),[22] tris(phenol),[23] tris(urea)[24] or tris(thiourea)[25] hydrogen-bonding moieties. The hydrogen-bonding complementarities with the tripodal hosts derived from tris(2-aminoethyl)amine resulted in binding affinities almost three orders of magnitude higher for $H_2PO_4^-$ (K = 14.2 × 10^3) compared to the similarly sized and charged HSO_4^- (K = 38). A large number of reports attest that urea is a very popular binding motif for kosmotropic tetrahedral anions, such as sulfate and phosphate. A large sulfate binding constant (K_a = 8.3 × 10^6), on a par with the sulfate-binding protein, has been achieved by a designed coordination cage containing six urea units.[17a] Besides tripodal urea-based receptors, a variety of other ligands containing multiple (up to six) urea moieties have been

reported.[26] Some of these urea-based ligands assemble into anion-binding hosts by coordinating to metals.[17a,27] Spherical anions, such as halides, were found to be extremely strongly bound by triazole-based macrocycles and cages (K_a = 10^{17}), exclusively via C–H hydrogen bonds.[28] Despite the wide variety of known examples, the search for better anion binding agents for specific applications continues due to various drawbacks. These include difficulty to synthesize and/or high cost, poor solubility, sensitivity to heat or low/high pH, weak binding affinity, poor selectivity, and poor recyclability.

The selective extraction of the sulfate anion from aqueous media has generated great interest in recent years, mostly aimed at the separation of sulfate from nuclear wastes[29] and seawater used for off-shore drilling.[30] While sulfate receptors with binding constants in H_2O (K_a = 8.6 × 10^9) three orders of magnitude higher than that of the SBP have been developed[31] and high selectivity for sulfate over anions with small hydration energy[32] such as NO_3^- ($\Delta G_h°$ = −289 kJ/mol), ClO_4^- ($\Delta G_h°$ = −229 kJ/mol) and Cl^- ($\Delta G_h°$ = −345 kJ/mol) has been achieved,[33] the selective binding and efficient extraction of sulfate in the presence of excess carbonate on a large scale is a particularly challenging problem that is yet to be realized.

Nanojars are a unique class of neutral anion receptors of the formula [anion{Cu^{II}(μ-OH)(μ-pz)}$_n$] (Cu_n; n = 27–33; pz = pyrazolate anion or a 4-substituted derivative) based on three [*cis*-Cu^{II}(μ-OH)(μ-pz)]$_m$ metallamacrocycles (m = 6–14, except 11) strongly connected to each other by an array of inter-metallamacrocycle and anion-metallamacrocycle hydrogen bonding as well as inter-metallamacrocycle Cu···O interactions. Nanojars display a number of distinctive features promoting their use as selective anion extraction agents.[34–42] First, they are easy to obtain by straightforward self-assembly from inexpensive, commercially available reagents. Second, they are soluble in most organic solvents and their solubility can be tuned by peripheral substitution to include both extremes of solvent polarity (long-chain aliphatic hydrocarbons and water). Third, they are thermally robust and do not decompose up to 200 °C. Fourth, nanojars display excellent resistance to highly alkaline conditions, allowing for the unprecedented liquid–liquid extraction of the highly hydrophilic CO_3^{2-} ion ($\Delta G°_h$ = −1324 kJ/mol) from a 10 M aqueous NaOH solution (pH > 14) into a long-chain aliphatic hydrocarbon solvent. Fifth, nanojars bind the incarcerated anions with exceptional strength, so that an aqueous Ba^{2+} solution is unable to precipitate the highly insoluble barium

salt of the incarcerated anion, when stirred with a solution of the corresponding nanojars. Sixth, nanojars are totally selective for hydrophilic anions with large hydration energies (PO_4^{3-}: $\Delta G_h° = -2773$ kJ/mol; CO_3^{2-}: $\Delta G°_h = -1324$ kJ/mol; HPO_4^{2-}: $\Delta G_h° = -1089$ kJ/mol; SO_4^{2-} $\Delta G_h° = -1064$ kJ/mol) over anions with small hydration energies.[32,43] Seventh, the incarcerated anion can easily be recovered from the nanojar host by slight acidification, offering recyclability.

Nanojars bear a striking resemblance to anion-binding proteins in that they both possess cavities lined by multiple hydrogen-bond donors that completely incarcerate and isolate the anion from the surrounding medium (Figure 1). Inspired by this similarity and guided by the knowledge that a judicious spatial arrangement of the H-bond donors is needed to achieve selectivity, we pursued the rigidification of the ligand backbone of nanojars by tethering pyrazole moieties together. Herein we present the synthesis of a series of tethered pyrazole ligands $HpzCH_2(CH_2)_xCH_2pzH$ (x = 0–4) (Scheme 1) and studies of their nanojar-forming ability, along with the effect of the tether length on the selectivity of the corresponding nanojars for sulfate vs. carbonate.

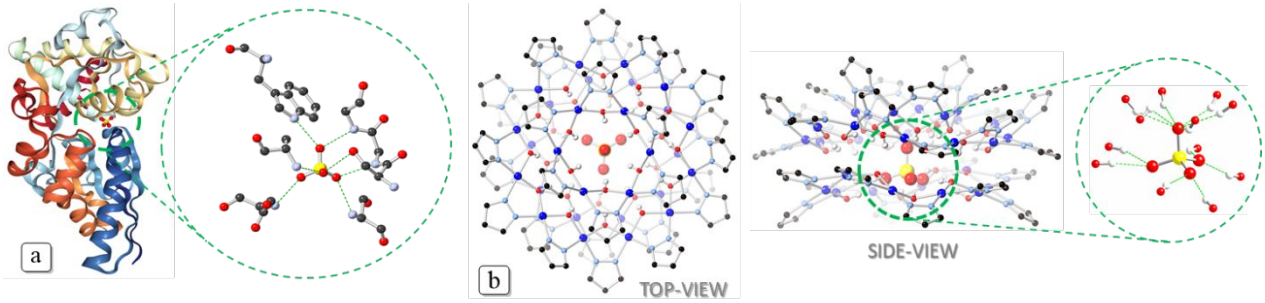

Figure 1. Illustration of the similarity between the binding pockets of anion-binding proteins (**a**: SBP of *Salmonella typhimurium*[3]) and nanojars (**b**: $[SO_4^{2-}\subset\{Cu(OH)(pz)\}_{28}]$;[35] color code: dark blue – Cu; light blue – N; red – O; black – C; light grey – H; C–H hydrogen atoms are not shown).

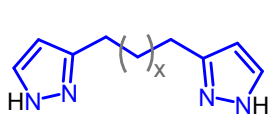

H_2**L2** (x = 0)
H_2**L3** (x = 1)
H_2**L4** (x = 2)
H_2**L5** (x = 3)
H_2**L6** (x = 4)

Scheme 1. The ligands used in this study.

2. Results and discussion

2.1. Synthesis of the new ligands

Tethered ligand 1,3-di(pyrazol-3(5)-yl)propane (H_2**L3**) was prepared in two steps starting with heptane-2,6-dione, which was reacted with dimethylformamide dimethylacetal (Scheme 2). The reaction of the resulting 1,9-bis(dimethylamino)nona-1,8-diene-3,7-dione intermediate (Figures S1 and S2) with hydrazine monohydrate produced H_2**L3** in an overall yield of 27% (Figures S3 and S4). The homologous ligands 1,4-di(pyrazol-3(5)-yl)butane (H_2**L4**) and 1,5-di(pyrazol-3(5)-yl)pentane (H_2**L5**) were also prepared in two steps, by a different, more convenient method (Scheme 2). *N*-Protected pyrazole was lithiated with ^{n}BuLi and then reacted with 1,4-diiodobutane or 1,5-diiodopentane. The resulting bis(1-(tetrahydropyran-2-yl)pyrazol-5-yl)alkane intermediates (Figures S5–S8) were then hydrolyzed to the corresponding ligands H_2**L4** and H_2**L5** in 67% and 63% overall yield, respectively (Figures S9–S12). This latter method was not convenient for the synthesis of H_2**L3**, because the reaction of (1-(tetrahydropyran-2-yl)pyrazol-5-yl)lithium with 1,3-diiodopropane (2:1 molar ratio) produced a mixture of products containing ~37% H_2**L3**, ~10% 5-iodo-1-(tetrahydropyran-2-yl)pyrazole and ~53% unreacted 1-(tetrahydropyran-2-yl)pyrazole (Figure S13). Also, when (1-(tetrahydropyran-2-yl)pyrazol-5-yl)lithium was reacted with 1,2-diiodoethane in a 4:1 molar ratio, partial iodination (14%) of the pyrazole 5-position was observed and no H_2**L2** formed (Figures S14 and S15). When the molar ratio employed was 1:2, nearly pure 5-iodo-1-(tetrahydropyran-2-yl)pyrazole was obtained with no sign of H_2**L2** formation (Figure S16). Although iodination of pyrazole by 1,2-diiodoethane or 1,3-diiodopropane has not been documented yet, iodination of similar substrates, such as indole,[44] imidazole[45] and benzimidazole[46] by 1,2-diiodoethane has been reported.

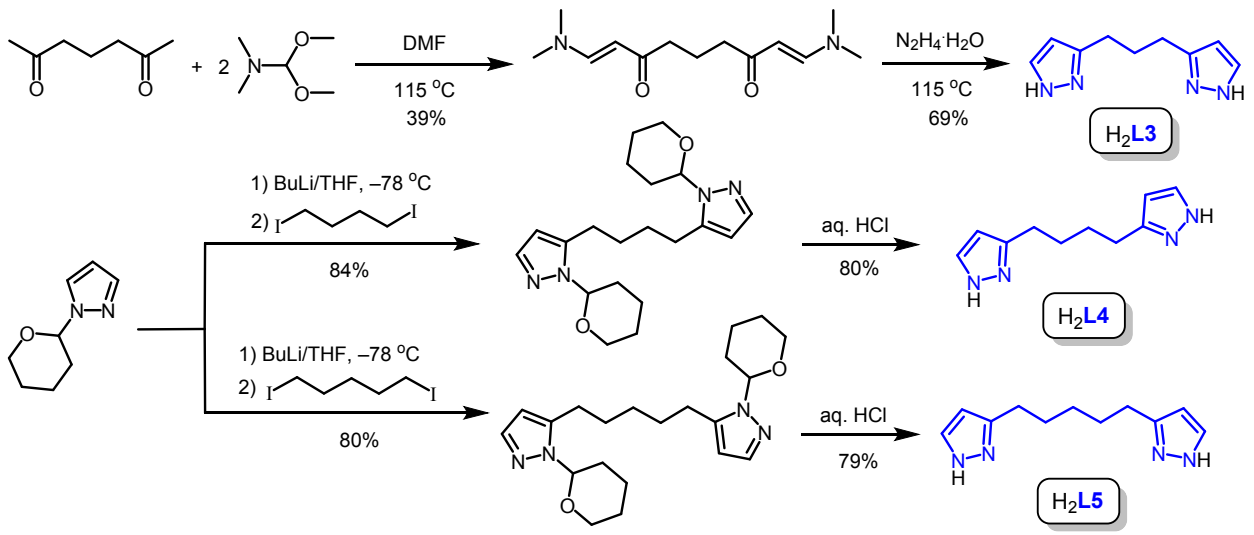

Scheme 2. Synthesis of the new ligands H_2**L3**, H_2**L4** and H_2**L5**.

2.2. Description of the crystal structures.

H_2**L4** is located on a general position within the triclinic (Pī) crystal lattice. One of the two pyrazole moieties of the ligand is approximately coplanar with the $(CH_2)_4$ unit, and forms a dihedral angle of 120.54(6)° with the second pyrazole unit (Figure 2). There are no significant π–π stacking interactions within the crystal lattice. Instead, the pyrazole units engage in edge-to-face, C–H···π interactions (centroid···centroid: 4.628(1) Å; (pz)H···pz(centroid): 2.617(1) Å) as well as several hydrogen bonds with each other (Table S1 and Figure S17). The closest centroid···centroid distance between parallel (crystallographically imposed) pyrazole moieties is 4.787(2) Å (plane separation: 3.699(2) Å). This pair of pz moieties related by an inversion center features C–H···π interactions with a $(pzCH_2)$H···pz(centroid) distance of 2.906(1) Å.

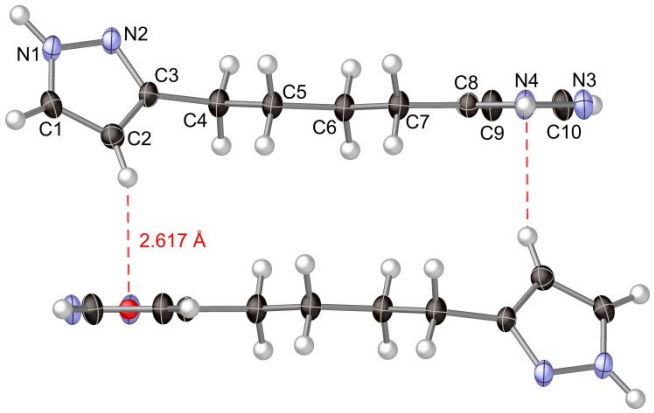

Figure 2. Thermal ellipsoid plot (50% probability) of **H_2L4** showing a pair of molecules symmetry-related by an inversion center. The red sphere illustrates the centroid of the pyrazole unit which is approximately coplanar with the $(CH_2)_4$ unit.

$(THP)_2$**L4** is located on an inversion center within the monoclinic ($P2_1/c$) crystal lattice (Figure 3). As opposed to H_2**L4**, the $pz(CH_2)_4pz$ moiety is planar in $(THP)_2$**L4**, and the pyrazole units are involved in columnar offset π–π stacking interactions (centroid···centroid: 4.646(1) Å; plane separation: 3.568(2) Å; dihedral angle: 0°) (Figure S18).

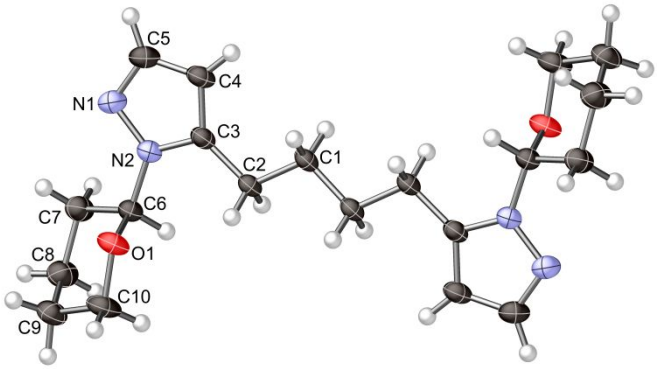

Figure 3. Thermal ellipsoid plot (50% probability) of the crystal structure of $(THP)_2$**L4** (only one position is shown for the disordered THP-moieties).

$(THP)_2$**L5** is located on a general position within the triclinic (Pī) crystal lattice (Figure 4). In contrast to $(THP)_2$**L4**, there are no significant aromatic interactions within the lattice; the closest centroid-centroid distance between parallel (crystallographically imposed) pyrazole planes is 5.412(1) Å (plane separation: 2.861(4) Å) (Figure S19).

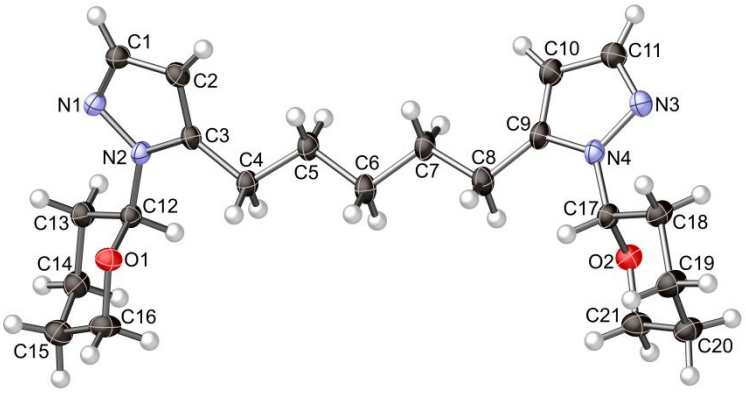

Figure 4. Thermal ellipsoid plot (50% probability) of the crystal structure of $(THP)_2$**L5**.

2.3. Formation of nanojars and tetranuclear complex

Depending on the ratio between copper nitrate, ligand H_2**L2** and base used for synthesis, either nanojars or two different tetranuclear complexes can be isolated.[47] Thus, the reaction of $Cu(NO_3)_2$, H_2**L2**, NaOH and Bu_4NOH in a 28:14:54:2 molar ratio in THF produces a mixture of nanojars in the presence of carbonate. ESI-MS(–) shows that the mixture contains $[CO_3{\subset}Cu_n(OH)_n(\mathbf{L2})_{n/2}]^{2-}$ (n = 26, *m/z* 2118; n = 28, *m/z* 2279; n = 30, *m/z* 2439) and $[CO_3{\subset}Cu_{28}(OH)_{27}(\mathbf{L2})_{14}(H\mathbf{L2})]^{2-}$ (*m/z* 2351). No nanojars form if $Cu(NO_3)_2$ is replaced by $CuSO_4$ and the reaction is carried out in the absence of carbonate. If the ratio between $Cu(NO_3)_2$, H_2**L2**, NaOH and Bu_4NOH is changed to 28:28:56:7, the tetranuclear complex $[Cu_4(\mu_4\text{-}OH)(\mu_3\text{-}\mathbf{L2})_4]^-$ (*m/z* 911) is obtained instead. Finally, if $Cu(NO_3)_2$, H_2**L2** and NaOH are used in a 28:14:42 molar ratio, a different tetranuclear complex, $[Cu_4(\mu_3\text{-}OH)_2(\mu_3\text{-}\mathbf{L2})_2(NO_3)_2]$ is obtained, which shows peaks at *m/z* 607 and 731 in the ESI-MS(+) and ESI-MS(–) spectra, corresponding to $[Cu_4O(OH)_2(\mathbf{L2})_2]^+$ and $[Cu_4O(OH)(\mathbf{L2})_2(NO_3)_2]^-$, respectively.

Because NaOH and $CuSO_4$ are not soluble in THF, we sought to explore whether using all soluble reagents would alter the outcome of the nanojar-forming reaction. First, a reaction using $Cu(NO_3)_2$, H_2**L2** and Bu_4NOH in a 28:14:58 molar ratio was carried out in THF (2 equiv. of Bu_4NOH react with atmospheric CO_2 to form $(Bu_4N)_2CO_3$ *in-situ*). ESI-MS(–)shows that the composition of the product mixture is significantly different from the one obtained with NaOH (Figure 5a). Thus, $[CO_3{\subset}Cu_{28}(OH)_{28}(\mathbf{L2})_{14}]^{2-}$ (*m/z* 2279) and $[CO_3{\subset}Cu_{30}(OH)_{30}(\mathbf{L2})_{15}]^{2-}$ (*m/z* 2439), which are the dominant species in the product

mixture obtained with NaOH, are absent in the one obtained with Bu_4NOH, and new species which were absent in the former, $[CO_3\subset Cu_{26}(OH)_{25}(\mathbf{L2})_{13}(H\mathbf{L2})]^{2-}$ (*m/z* 2190) and $[CO_3\subset Cu_{29}(OH)_{30}(\mathbf{L2})_{14}]^{2-}$ (*m/z* 2328) are present in the latter along with $[CO_3\subset Cu_{26}(OH)_{26}(\mathbf{L2})_{13}]^{2-}$ (*m/z* 2118) and $[CO_3\subset Cu_{28}(OH)_{27}(\mathbf{L2})_{14}(H\mathbf{L2})]^{2-}$ (*m/z* 2351), which are present in both.

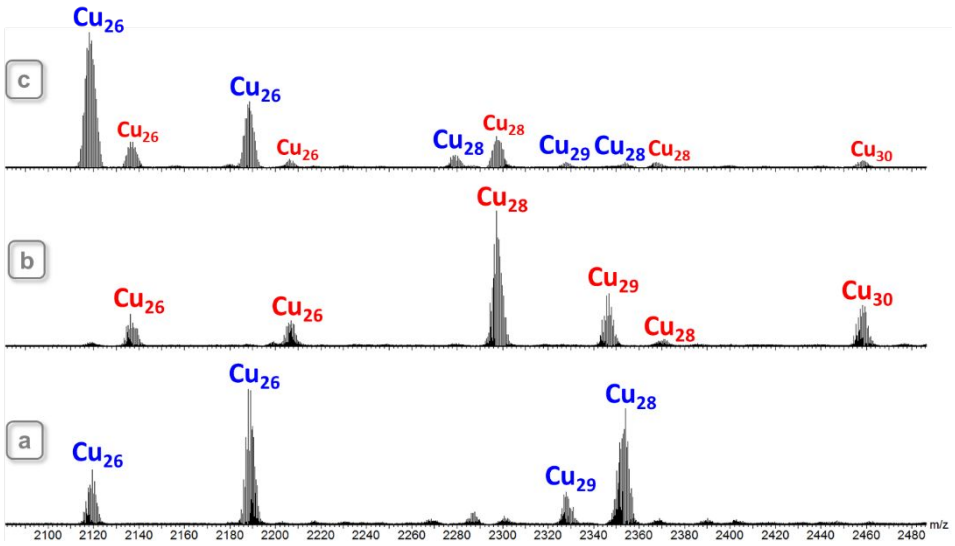

Figure 5. ESI-MS(–) spectra in CH_3CN of the nanojar mixtures formed by **L2** with (a) CO_3^{2-}, (b) SO_4^{2-}, and (c) a mixture of CO_3^{2-} and SO_4^{2-} (1:1 molar ratio). Cu_n abbreviations show the nuclearity of the nanojars with CO_3^{2-} (blue) or SO_4^{2-} (red); assignments are described in the text.

A very different outcome is observed when THF-soluble $(Bu_4N)_2SO_4$ is used instead of $CuSO_4$ as the sulfate ion source for nanojar formation with $H_2\mathbf{L2}$. While no SO_4-nanojars can be obtained from $CuSO_4$, $H_2\mathbf{L2}$, NaOH and Bu_4NOH in a 28:14:54:2 molar ratio in THF, the reaction of $Cu(NO_3)_2$, $H_2\mathbf{L2}$, Bu_4NOH and Bu_4NHSO_4 in a 28:14:84:28 molar ratio ($(Bu_4N)_2SO_4$ forms *in-situ*) produces a SO_4-nanojar mixture analogous to the CO_3-nanojar mixture obtained with $(Bu_4N)_2CO_3$ (Figure 5b). The major difference observed is that in addition to $[SO_4\subset Cu_{26}(OH)_{26}(\mathbf{L2})_{13}]^{2-}$ (*m/z* 2136), $[SO_4\subset Cu_{26}(OH)_{25}(\mathbf{L2})_{13}(H\mathbf{L2})]^{2-}$ (*m/z* 2208), $[SO_4\subset Cu_{29}(OH)_{30}(\mathbf{L2})_{14}]^{2-}$ (*m/z* 2346) and $[SO_4\subset Cu_{28}(OH)_{27}(\mathbf{L2})_{14}(H\mathbf{L2})]^{2-}$ (*m/z* 2369), of which analogs have been observed with carbonate, $[SO_4\subset Cu_{28}(OH)_{28}(\mathbf{L2})_{14}]^{2-}$ (*m/z* 2297) and $[SO_4\subset Cu_{30}(OH)_{30}(\mathbf{L2})_{15}]^{2-}$ (*m/z* 2458) are also present.

The new ligand **L3**, which has a longer propylene tether (vs. ethylene in **L2**) between the two pyrazole moieties, is also accommodated in homoleptic nanojars. ESI-MS(–) of the

product mixture obtained from $Cu(NO_3)_2$, H_2**L3** and Bu_4NOH in a 28:14:58 molar ratio in THF in the presence of atmospheric CO_2 indicates the formation of $[CO_3{\subset}Cu_{26}(OH)_{26}(\mathbf{L3})_{13}]^{2-}$ (*m/z* 2209), $[CO_3{\subset}Cu_{28}(OH)_{28}(\mathbf{L3})_{14}]^{2-}$ (*m/z* 2377), $[CO_3{\subset}Cu_{28}(OH)_{26}(\mathbf{L3})_{15}]^{2-}$ (*m/z* 2447) and $[CO_3{\subset}Cu_{30}(OH)_{30}(\mathbf{L3})_{15}]^{2-}$ (*m/z* 2545) (Figure 6a). When the reaction is carried out with NaOH as base and $Cu(NO_3)_2$, H_2**L3**, NaOH and $(Bu_4N)_2CO_3$ in a 28:14:54:2 molar ratio, a mixture with a slightly different nanojar distribution is obtained (Figure S20). The corresponding SO_4-incarcerating nanojar mixture, obtained from the reaction of $Cu(NO_3)_2$, H_2**L3**, Bu_4NOH and Bu_4NHSO_4 in a 28:14:84:28 molar ratio, is similar to the CO_3-analogs, with ESI-MS(–) peaks corresponding to $[SO_4{\subset}Cu_{26}(OH)_{26}(\mathbf{L3})_{13}]^{2-}$ (*m/z* 2228), $[SO_4{\subset}Cu_{28}(OH)_{28}(\mathbf{L3})_{14}]^{2-}$ (*m/z* 2395), $[SO_4{\subset}Cu_{28}(OH)_{26}(\mathbf{L3})_{15}]^{2-}$ (*m/z* 2465) and $[SO_4{\subset}Cu_{30}(OH)_{30}(\mathbf{L3})_{15}]^{2-}$ (*m/z* 2563) (Figure 6b).

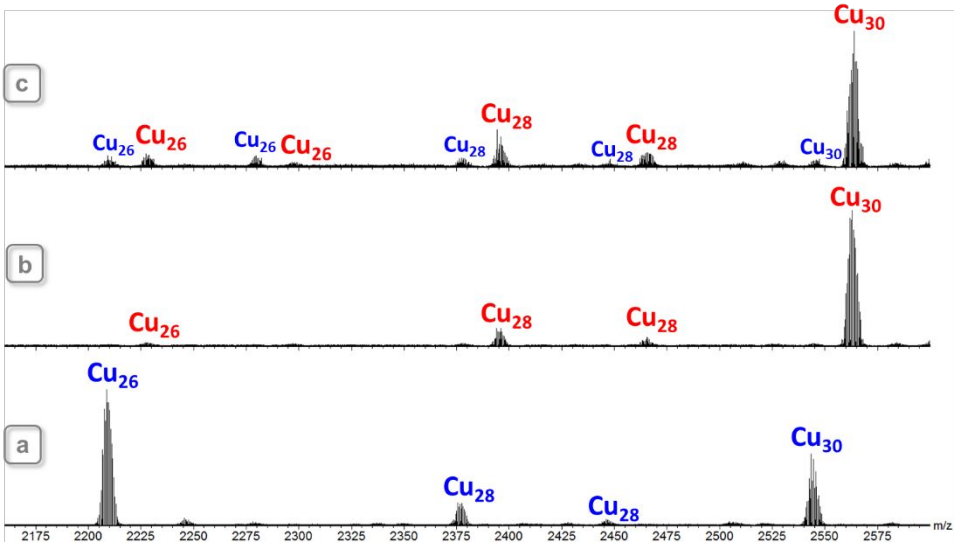

Figure 6. ESI-MS(–) spectra in CH_3CN of the nanojar mixtures formed by **L3** with (a) CO_3^{2-}, (b) SO_4^{2-} and (c) a mixture of CO_3^{2-} and SO_4^{2-} (1:1 molar ratio). Cu_n abbreviations show the nuclearity of the nanojars with CO_3^{2-} (blue) or SO_4^{2-} (red); assignments are described in the text.

As with H_2**L2**, a tetranuclear complex $[Cu_4(OH)_2(\mathbf{L3})_2(NO_3)_2]$ can also be obtained from the reaction of $Cu(NO_3)_2$, H_2**L3** and NaOH in a 28:14:42 molar ratio. The ESI-MS(–) spectrum shows peaks at *m/z* 733 and 760, corresponding to $[Cu_4(OH)_4(\mathbf{L3})_2(NO_3)]^-$ and $[Cu_4O(OH)(\mathbf{L3})_2(NO_3)_2]^-$, respectively (Figure S21). However, a complex analogous to $[Cu_4(OH)(\mathbf{L2})_4]^-$ cannot be obtained with H_2**L3**. Instead, the reaction of $Cu(NO_3)_2$, H_2**L3** and

Bu_4NOH in a 28:28:63 molar ratio produces the nanojar $[CO_3{\subset}Cu_{26}(OH)_{26}(\mathbf{L3})_{13}]^{2-}$ (*m/z* 2209) in almost pure form (Figure S22).

When the tether between the two pyrazole moieties becomes longer than $-(CH_2)_3-$, no homoletic nanojars can be obtained. However, when a 1:2 molar mixture of **L4**–**L6** and pyrazole (Hpz) is employed, heteroleptic nanojars can be obtained. Within each Cu_n group, up to 7–8 tethered ligands are incorporated into the nanojars, while the average number of **L4**–**L6** ligands per nanojar is 5.

ESI-MS(–) shows that the product obtained from the reaction of $Cu(NO_3)_2$, H_2**L4**, Hpz and Bu_4NOH in a 28:7:14:58 molar ratio in THF in the presence of atmospheric CO_2 contains $[CO_3{\subset}Cu_n(OH)_n(\mathbf{L4})_y(pz)_{n-2y}]^{2-}$ (n = 27, y = 1–7, *m/z* 2050–2212; n = 29, y = 3–7, *m/z* 2252–2360; n = 30, y = 4–6, *m/z* 2353–2407; n = 31, y = 2–8, *m/z* 2372–2535) (Figure 7). When the reaction is carried out with $Cu(NO_3)_2$, H_2**L4**, Hpz, Bu_4NOH and $(Bu_4N)_2SO_4$ in a 28:7:14:56:1 molar ratio, the corresponding sulfate nanojars are obtained: $[SO_4{\subset}Cu_n(OH)_n(\mathbf{L4})_y(pz)_{n-2y}]^{2-}$ (n = 27, y = 3–6, *m/z* 2122–2203; n = 28, y = 5–7, *m/z* 2250–2304; n = 29, y = 3–7, *m/z* 2270–2378; n = 31, y = 2–8, *m/z* 2390–2553) (Figure S23). With both CO_3^{2-} and SO_4^{2-}, the abundance of the different nanojar sizes increases in the order $Cu_{27} < Cu_{29} < Cu_{31}$ (traces of Cu_{30} and Cu_{28} nanojars are also observed with CO_3^{2-} and SO_4^{2-}, respectively).

The distribution of the corresponding nanojar species obtained with **L5**/pz (1:2) and carbonate, $[CO_3{\subset}Cu_n(OH)_n(\mathbf{L5})_y(pz)_{n-2y}]^{2-}$ (n = 27, y = 1–5, *m/z* 2057–2193; n = 28, y = 4, *m/z* 2233; n = 29, y = 2–5, *m/z* 2239–2341; n = 30, y = 4–7, *m/z* 2381–2483; n = 31, y = 4–7, *m/z* 2454–2557) (Figure S24), is different than in the case of **L4**/pz. Thus, while present only in traces with **L4**/pz, Cu_{30} nanojars are the dominant species with **L5**/pz. The abundance of different sizes follows the order: $Cu_{27} \approx Cu_{31} < Cu_{29} < Cu_{30}$. The distribution of the sulfate-analogs, $[SO_4{\subset}Cu_n(OH)_n(\mathbf{L5})_y(pz)_{n-2y}]^{2-}$ (n = 27, y = 2–6, *m/z* 2109–2245; n = 29, y = 3–7, *m/z* 2291–2427; n = 30, y = 5–9, *m/z* 2433–2569; n = 31, y = 3–10, *m/z* 2438–2677) (Figure S25), is also different than in the case of **L4**/pz. Here, the dominant species are Cu_{29} and Cu_{30} (as with carbonate) and only small amounts of Cu_{27} and Cu_{31} species are observed.

In the case of **L6**/pz (1:2) with carbonate, the distribution of the nanojar species is similar to the one obtained with **L5**/pz, with the notable difference that the Cu_{28} species are significantly more abundant: $[CO_3{\subset}Cu_n(OH)_n(\mathbf{L6})_y(pz)_{n-2y}]^{2-}$ (n = 27, y = 1–6, *m/z*

2064–2269; n = 28, y = 3–8, *m/z* 2220–2425; n = 29, y = 3–6, *m/z* 2294–2417; n = 30, y = 4–7, *m/z* 2409–2532; n = 31, y = 5–7, *m/z* 2524–2606) (Figure S26). As with **L5**/pz, the Cu_{30} nanojars are the dominant species; the abundance of different sizes increases in the order: Cu_{31} < Cu_{27} ≈ Cu_{28} ≈ Cu_{29} < Cu_{30}. The distribution of the sulfate-analogs, $[SO_4{\subset}Cu_n(OH)_n(\mathbf{L6})_y(pz)_{n-2y}]^{2-}$ (n = 27, y = 3–6, *m/z* 2164–2287; n = 28, y = 4–7, *m/z* 2279–2402; n = 29, y = 3–7, *m/z* 2312–2476; n = 30, y = 5–8, *m/z* 2468–2591) (Figure S27), is significantly different from the one obtained with **L5**. Whereas Cu_{31} nanojars were the dominant species with **L4**, they are absent with **L6**, and Cu_{28} species are observed instead (which were absent with **L5**, and present in very small amounts with **L4**). The dominant species with **L6**/pz are Cu_{30}, and the abundance of different sizes follows the order: Cu_{27} ≈ Cu_{28} < Cu_{29} < Cu_{30}. In addition to these nanojar species, a few peaks corresponding to $[SO_4{\subset}Cu_{22}(OH)_{22}(\mathbf{L6})_y(pz)_{22-2y}]^{2-}$ (y = 6, *m/z* 1918; y = 7, *m/z* 1959; y = 8, *m/z* 2000) and hitherto unidentified species at m/z 3094 and 3175 are observed (Figure S28).

Although not verified experimentally, ligand **L1** ($pzCH_2pz$) is not expected to form nanojars due to the very short tether which places the pyrazole moieties too close to each other to allow for the assembly of the different $[cis\text{-}Cu^{II}(\mu\text{-}OH)(\mu\text{-}pz)]_m$ metallamacrocycles needed for nanojar formation.

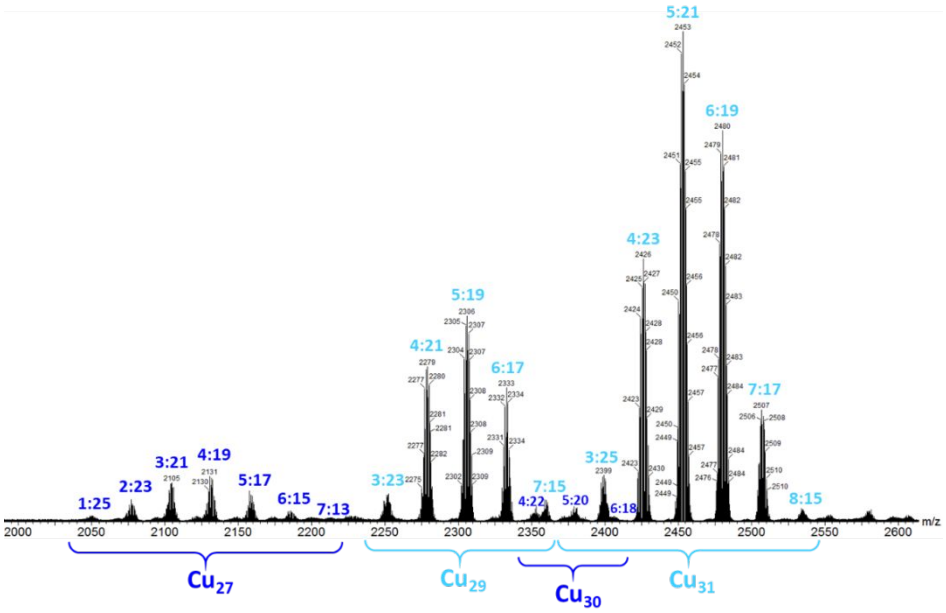

Figure 7. ESI-MS(–) spectrum in CH_3CN of the nanojar mixture $[CO_3{\subset}Cu_n(OH)_n(\mathbf{L4})_y(pz)_{n-2y}]^{2-}$ formed by **L4** in mixture with pz (1:2 molar ratio) with carbonate. Cu_n abbreviations show the nuclearity of the nanojars, and the molar ratio between **L4** and pz in a given nanojar is indicated by y:n–2y.

Similarly to nanojars based on the parent pyrazole ligand, nanojars with tethered pyrazoles are also stable to heating in a THF solution to 66 °C (the boiling point of the solvent), as indicated by ESI-MS spectrometry.

2.4. Selectivity studies on CO_3^{2-} vs. SO_4^{2-} incarceration by nanojars formed with tethered pyrazole ligands

While nanojars based on the parent pyrazole ligand (pz) are totally selective for CO_3^{2-} or SO_4^{2-} (anions with large hydration energies) over NO_3^-, ClO_4^-, BF_4^-, Cl^-, Br^- and I^- (anions with small hydration energies), they offer no selectivity between CO_3^{2-} and SO_4^{2-}. As shown in Figure S29, an approximately equal abundance of carbonate- and sulfate-incarcerating nanojars are obtained with Hpz when the reaction medium contains equimolar amounts of carbonate and sulfate. We hypothesized that tethering pairs of pyrazole moieties together will rigidify the nanojar outer shell, which in turn will limit the possible orientations of the inner OH hydrogen-bond donors surrounding the incarcerated anion and will lead to selectivity. As indicated by crystal structures,[35–39,48] the position and relative orientation of the OH groups lining the inner cavity of nanojars is related to the position of the pyrazole ligands coordinated to the same Cu-center, which has a distorted square-planar coordination geometry with two *cis*-pz and two *cis*-OH ligands. Thus, a tether between neighboring pyrazole ligands is expected to alter the relative orientation of the pyrazole moieties, and consequently the position of the corresponding OH groups.

Selectivity studies for carbonate vs. sulfate were carried out with both H_2**L2** and H_2**L3** in THF solution containing $Cu(NO_3)_2$ and the tethered ligand in a 2:1 molar ratio, to which a THF solution containing equimolar amounts of $(Bu_4N)_2CO_3$ and $(Bu_4N)_2SO_4$, as well as the required amount of Bu_4NOH base was added under vigorous stirring. The resulting nanojar mixtures were precipitated out by pouring the reaction solution into excess water, and were analyzed using mass spectrometry. The relative amounts of different nanojar species obtained are shown in Table 1. As predicted, selectivity is observed in both cases.

In the case of **L2**, ESI-MS(−) shows that overall the obtained nanojars strongly favor carbonate (Figure 5c). In contrast, the nanojars obtained with **L3** overall strongly favor sulfate (Figure 6c). It is noteworthy that in the case of **L2** the overwhelmingly dominant nanojar size in the mixture is Cu_{26}, whereas in the case of **L3** the overwhelmingly dominant

nanojar size is Cu_{30}. This observation can be corroborated with the size difference between carbonate (average C–O bond length: 1.28 Å) and sulfate (average S–O bond length: 1.48 Å). Thus, the smaller carbonate ion prefers the smaller Cu_{26} nanojar, whereas the larger sulfate ion prefers the larger Cu_{30} nanojar. It is also evident that the ligand with shorter tether, **L2** favors the smaller Cu_{26} nanojar (no Cu_{30} nanojar is observed with carbonate; Figure 5), while the ligand with longer tether, **L3** favors the larger Cu_{30} nanojar (Cu_{30} is by far the most abundant nanojar obtained with sulfate; Figure 6).

Table 1. Summary of the various homoleptic (**L** = **L2** and **L3**) or heteroleptic (**L** = **L4**–**L6**; pz = pyrazolate) nanojar species observed in selectivity experiments using a 1:1 molar mixture of CO_3^{2-} and SO_4^{2-}. Heteroleptic nanojars were obtained using a 1:2 molar mixtures of H**L4**–H**L6** and Hpz (see Figures S30–S32 for the observed values of y). For each given ligand, values in the corresponding columns indicate relative amounts of different nanojar species observed by ESI-MS(–).

NANOJAR	**L2**		**L3**		**L4**/pz		**L5**/pz		**L6**/pz	
	CO_3^{2-}	SO_4^{2-}	CO_3^{2-}	SO_4^{2-}	CO_3^{2-}	SO_4^{2-}	CO_3^{2-}	SO_4^{2-}	CO_3^{2-}	SO_4^{2-}
$[anion\subset Cu_{26}(OH)_{26}(\mathbf{L})_{13}]^{2-}$	50.9	8.7	2.5	3.4	–	–	–	–	–	–
$[anion\subset Cu_{26}(OH)_{25}(\mathbf{L})_{13}(H\mathbf{L})]^{2-}$	21.5	1.7	–	–	–	–	–	–	–	–
$[anion\subset Cu_{26}(OH)_{24}(\mathbf{L})_{14}]^{2-}$	–	–	2.6	1.4	–	–	–	–	–	–
$[anion\subset Cu_{27}(OH)_{27}(\mathbf{L})_{y}(pz)_{27-2y}]^{2-}$	*n/a*	*n/a*	*n/a*	*n/a*	20.7	1	–	–	90.1	33.2
$[anion\subset Cu_{28}(OH)_{28}(\mathbf{L})_{14}]^{2-}$	3.6	9.7	2.3	6.9	–	–	–	–	–	–
$[anion\subset Cu_{28}(OH)_{27}(\mathbf{L})_{14}(H\mathbf{L})]^{2-}$	1	1.3	–	–	–	–	–	–	–	–
$[anion\subset Cu_{28}(OH)_{26}(\mathbf{L})_{15}]^{2-}$	–	–	1	4.3	–	–	–	–	–	–
$[anion\subset Cu_{28}(OH)_{28}(\mathbf{L})_{y}(pz)_{28-2y}]^{2-}$	*n/a*	*n/a*	*n/a*	*n/a*	–	–	12.8	–	108.4	12.2
$[anion\subset Cu_{29}(OH)_{30}(\mathbf{L})_{14}]^{2-}$	1.1	1.8	–	–	–	–	–	–	–	–
$[anion\subset Cu_{29}(OH)_{29}(\mathbf{L})_{y}(pz)_{29-2y}]^{2-}$	*n/a*	*n/a*	*n/a*	*n/a*	54.2	1.3	6.4	1	1	8.3
$[anion\subset Cu_{30}(OH)_{30}(\mathbf{L})_{15}]^{2-}$	–	–	1.7	33.0	–	–	–	–	–	–
$[anion\subset Cu_{30}(OH)_{30}(\mathbf{L})_{y}(pz)_{30-2y}]^{2-}$	*n/a*	*n/a*	*n/a*	*n/a*	8.3	–	17.0	2.1	13.3	6.0
$[anion\subset Cu_{31}(OH)_{31}(\mathbf{L})_{y}(pz)_{31-2y}]^{2-}$	*n/a*	*n/a*	*n/a*	*n/a*	15.0	3.1	–	–	–	–
OVERALL (relative amounts)	3.4	1	1	4.9	18.3	1	11.8	1	3.6	1

Because homoleptic nanojars could not be obtained with **L4**–**L6**, selectivity studies were carried out using 1:2 molar mixtures of H**L4**–H**L6** and pyrazole (Hpz). The resulting heteroleptic nanojars strongly favor carbonate with **L4** and **L5**, and moderately favor carbonate with **L6** (Table 1).

In the case of **L4**/pz (1:2), the ESI-MS(–) spectrum of the nanojar mixture closely resembles the one of the nanojars obtained using carbonate only, with only traces of the corresponding sulfate-analogs (Figure S30). In terms of distribution of the different nanojar sizes, the only noticeable difference between the two spectra is that in the one obtained with

the CO_3^{2-}/SO_4^{2-} (1:1) mixture, the abundance of the Cu_{31} nanojars is much lower than in the one obtained with CO_3^{2-} only.

The ESI-MS(–) spectrum of the nanojar mixture obtained with **L5**/pz (1:2) and CO_3^{2-}/SO_4^{2-} (1:1) also resembles the one with CO_3^{2-} alone, with the major difference that Cu_{27} and Cu_{31} species are virtually absent and Cu_{28} nanojars are present in significant amounts (only small amounts were observed with carbonate alone). Again, only traces of the corresponding sulfate-analogs are present (Figure S31).

A quite different scenario is observed in the case of **L6**/pz (1:2). While sulfate-nanojars were only seen in traces with **L4** and **L5**, they are present in much more significant amounts with **L6**, although the carbonate-analogs are still dominant (except the for the Cu_{29} species) (Figure S32). Also, the abundance of Cu_{30} species is much lower than in the mixture obtained with carbonate only.

All pyrazole-based ligands described above, as well as the incarcerated anions can be recycled by acidification of the nanojar solution. As described before,[40] protonation of the pyrazolate moieties leads to the disruption of the nanojar scaffold and release of the incarcerated anion. The ligand can be recycled by addition of a base, which leads to the re-assembly of the nanojar.

3. Conclusions

While selective binding of oxyanions with large hydration energies (CO_3^{2-}, SO_4^{2-}, HPO_4^{2-}) in the presence of oxyanions with small hydration energies (NO_3^-, ClO_4^-) is an inherent property of nanojars, the selective binding of a highly hydrophilic oxyanion by nanojars in the presence of another highly hydrophilic oxyanion is a much more challenging task. Nanojars based on the parent pyrazole (pz) ligand have a rather flexible outer shell and inner anion binding cavity; therefore, they bind CO_3^{2-} and SO_4^{2-} with the same propensity. By using a series of homologous ligands, $^-pzCH_2(CH_2)_xCH_2pz^-$ (x = 0–4; **L2**–**L6**), we have demonstrated that the rigidification of the nanojar outer shell by tethering pairs of pyrazole moieties together results in selectivity either for carbonate (with **L2** and with **L4**–**L6**/pz mixtures) or for sulfate (with **L3**). Depending on the tether length, either homoleptic (with **L2** and **L3**, y = n/2) or heteroleptic (with **L4**–**L6**, y < n/2) nanojars of the formula

$(Bu_4N)_2$[anion⊂$Cu_n(OH)_n$(**L2**–**L6**)$_y(pz)_{n-2y}$] (n = 26–31) have been obtained. Although most homoleptic nanojars observed are represented by the formula $(Bu_4N)_2$[anion⊂$Cu_n(OH)_n$(**L2**/**L3**)$_{n/2}$] (n = 26, 28, 30), three additional types of species have also been observed. In one, *n* is an even number and an OH^- group is replaced by a pyrazolate moiety of an additional monoprotonated tethered ligand: $(Bu_4N)_2$[anion⊂$Cu_n(OH)_{n-1}$(**L2**)$_{n/2}$(H**L2**)]; in another, described by the formula $(Bu_4N)_2$[anion⊂$Cu_n(OH)_{n+1}$(**L2**)$_{(n-1)/2}$], n is an odd number. Finally, species in which two OH^- groups are replaced by an additional tethered ligand are observed with **L3**: $(Bu_4N)_2$[anion⊂$Cu_n(OH)_{n-2}$(**L3**)$_{(n/2)+1}$] (n is an even number). None of these species have been observed in significant amounts in heteroleptic nanojar mixtures.

It is apparent that nanojars are not required to be homoleptic to achieve high selectivity for CO_3^{2-} over SO_4^{2-}, as heteroleptic nanojars incorporating ~5 tethered ligands (**L4** or **L5**) on average offer even higher selectivity than the homoleptic nanojar obtained with **L2** alone. On the other hand, only homoleptic nanojars based on **L3** are selective for sulfate.

Nanojars (5–6 kDa) are larger than most known artificial anion extraction agents; yet, they offer the possibility of creating anion binding pockets similar to those in highly selective anion-binding proteins (30–40 kDa). The growth of single-crystals of rigidified nanojars suitable for X-ray diffraction studies using conventional techniques has not been straightforward, likely due to various possible positions and conformations of the tethers. Crystal growing efforts, using not only different crystallization conditions but also various different counterions or additives for co-crystallization, is currently underway. Structural details of the binding of different anions by nanojars with rigidified outer shells will allow for the rationalization of the observed selectivities, which in turn will guide future efforts to further increase selectivity and to achieve selectivity for other anions as well.

4. Experimental section

Materials and methods

All commercially available chemicals were used as received. Heptane-2,6-dione,[49] 1-(tetrahydropyran-2-yl)pyrazole,[50] 1,2-bis(pyrazol-3(5)-yl)ethane[47] and 1,6-bis(pyrazol-

3(5)-yl)hexane[50] were prepared according to published procedures. THF was dried with Na/benzophenone, and deionized water was boiled then cooled and stored under an N_2 atmosphere. UV-vis and NMR spectra were collected on a Shimadzu UV-1650PC spectrophotometer and a Jeol JNM-ECZS (400 MHz) instrument, respectively.

Synthesis of 1,9-bis(dimethylamino)nona-1,8-diene-3,7-dione.

A solution of heptane-2,6-dione (6.300 g, 49.19 mmol) and dimethylformamide dimethylacetal (DMF-DMA; 41.298 g, 346.6 mmol) in dimethylformamide (DMF; 65 mL) is refluxed in a 250 mL round-bottom flask at 115 °C for 24 hours. The color of the solution gradually turns yellow and finally dark orange. The excess DMF-DMA and the DMF solvent are distilled out under high-vacuum with heating on a water bath (at ~60 °C). The viscous, dark orange/brown oily residue (10.301 g) is purified by column chromatography on silica gel (750 g) using EtOAc/MeOH gradient elution (9:1, 8:2, 7:3, 2:1, 1:1; the corresponding R_f values are 0.05, 0.13, 0.26, 0.29, 0.39). The product is obtained as a dark orange viscous oil (yield: 4.573 g, 39%). ^{1}H NMR (400 MHz, $CDCl_3$): δ 7.51 (d, 2H, *J* = 13 Hz, =C*H*), 5.03 (d, 2H, *J* = 13 Hz, =C*H*), 3.03 (s, br, 6H, N(CH_3)$_2$), 2.79 (s, br, 6H, N(CH_3)$_2$), 2.37 (t, 4H, *J* = 7.5 Hz, CH_2CH$_2$CH_2), 1.92 (p, 2H, *J* = 7.5 Hz, CH$_2$CH_2CH$_2$) ppm. ^{13}C NMR (101 MHz, $CDCl_3$): δ 198.2, 152.6, 96.1, 44.9, 41.0, 37.1, 22.4 ppm. HRMS (ESI-TOF) *m/z*: $[M+Na]^+$ calcd. for $C_{13}H_{22}N_2NaO_2$ 261.1579; found 261.1526.

Synthesis of 1,3-bis(1*H*-pyrazole-3(5)-yl)propane (H_2L3).

1,9-Bis(dimethylamino)nona-1,8-diene-3,7-dione (4.018 g, 16.86 mmol) is dissolved in ethanol (200 mL) and hydrazine monohydrate (3.17 mL, 3.27 g, 65.4 mmol) is added. After refluxing for 6 hours, the dark orange solution is boiled with activated carbon for 30 minutes and is then filtered while hot. The solvent is removed under vacuum and ligand **H_2L3** is obtained as a light-orange, extremely viscous oil (yield: 2.035 g, 69%). ^{1}H NMR (400 MHz, DMSO-d_6): δ 12.47 (s, br, 2H, N*H*), 7.45 (s, 2H, 5-*H*-pz), 6.04 (s, 2H, 4-*H*-pz), 2.59 (t, 4H, *J* = 7.6 Hz, CH_2CH$_2$CH_2), 1.88 (p, 2H, ^3J = 7.6 Hz, CH$_2$CH_2CH$_2$) ppm. ^{13}C NMR (101 MHz, DMSO-d_6): δ 147.1, 134.6, 103.4, 29.6, 26.4 ppm. HRMS (ESI-TOF) *m/z*: $[M+Na]^+$ calcd. for $C_9H_{12}N_4Na$ 199.0960; found 199.0434.

General procedure for the synthesis of bis(1-(tetrahydropyran-2-yl)pyrazol-5-yl)alkanes.

1-(Tetrahydropyran-2-yl)pyrazole (5.000 g, 32.85 mmol) is added to a 100 mL three-necked round bottom flask equipped with a pressure-equalizing addition funnel and a stir bar. The flask is purged with N_2 and anhydrous THF (50 mL) is added under stirring. Then, the flask is cooled to −78 °C in a dry-ice/isopropanol bath and *n*-butyllithium (1.6 M in hexanes, 21 mL, 33 mmol) is added dropwise from the addition funnel to the solution under stirring. The reaction mixture is stirred for 30 minutes at −78 °C. Then, 1,4-diiodobutane or 1,5-diiodopentane (10.95 mmol) is added dropwise from an N_2-purged syringe over 20 minutes. After stirring at −78 °C for 3 hours, the reaction solution is allowed to warm up to room temperature and is carefully quenched with water (1 mL). The volatiles are removed under reduced pressure, water (80 mL) is added to the residue, followed by extraction with ethyl acetate (3 × 80 mL). The combined organic layers are washed with brine (80 mL) and dried over anhydrous $MgSO_4$. After filtration, ethyl acetate is removed under reduced pressure, and the residue is recrystallized from ethyl acetate/hexanes.

1,4-Bis(1-(tetrahydropyran-2-yl)pyrazol-5-yl)butane. White solid. Yield: 4.946 g (84%) ^{1}H NMR (400 MHz, $CDCl_3$): δ 7.45 (s, 2H, 3-*H*-pz), 6.04 (s, 2H, 4-*H*-pz), 5.22 (d, 2H, C*H*-THP, *J* = 9.6 Hz), 4.00 (d, 2H, CH_2O-THP, *J* = 11.6 Hz), 3.59 (t, 2H, CH_2O-THP, J = 10.8 Hz), 2.75-2.63 (m, 4H, CH_2(CH_2)$_2$CH_2), 2.53-2.44 (m, 2H, CH_2-THP), 2.11-2.08 (m, 2H, CH_2-THP), 1.93 (d, 2H, CH_2-THP, *J* = 13.2 Hz), 1.75-1.55 (m, 10H, 3CH_2-THP and CH_2CH_2C$H_2$$CH_2$) ppm. ^{13}C NMR (400 MHz, $CDCl_3$): δ 143.37, 139.13, 105.05, 84.26, 67.78, 29.54, 28.15, 25.09, 25.03, 22.95 ppm. HRMS (ESI-TOF) *m*/*z*: $[M+Na]^+$ calcd for $C_{20}H_{30}N_4NaO_2$ 381.2267; found 381.2267.

1,5-Bis(1-(tetrahydropyran-2-yl)pyrazol-5-yl)pentane. Colorless solid. Yield: 4.895 g (80%). ^{1}H NMR (400 MHz, $CDCl_3$): δ 7.45 (s, 2H, 3-*H*-pz), 6.03 (s, 2H, 4-*H*-pz), 5.23 (d, 2H, C*H*-THP, *J* = 10 Hz), 4.01 (d, 2H, CH_2O-THP, *J* = 11.6 Hz), 3.61 (t, 2H, CH_2O-THP, *J* = 10.6 Hz), 2.73-2.60 (m, 4H, CH_2(CH_2)$_3$CH_2), 2.54-2.45 (m, 2H, CH_2-THP), 2.11-2.08 (m, 2H, CH_2-THP), 1.93 (d, 2H, CH_2-THP, *J* = 13.2 Hz), 1.72-1.55 (m, 10H, 3CH_2-THP and CH_2C$H_2$$CH_2CH_2$$CH_2$), 1.50-1.43 (m, 2H, ($CH_2$)$_2CH_2$($CH_2$)$_2$) ppm. ^{13}C NMR (400 MHz, $CDCl_3$): δ 143.67, 139.14, 104.98, 84.23, 67.82, 29.56, 28.96, 28.37, 25.17, 25.09, 22.99 ppm. HRMS (ESI-TOF) *m*/*z*: $[M+Na]^+$ calcd for $C_{21}H_{32}N_4NaO_2$ 395.2423; found 395.2426.

General procedure for the synthesis of bis(pyrazol-3(5)-yl)alkanes.

Bis(1-(tetrahydropyran-2-yl)pyrazol-5-yl)alkane (13.00 mmol) is dissolved in ethanol (130 mL) and conc. HCl (37%; 6.5 mL) is added dropwise under stirring. The reaction mixture is

stirred at room temperature for 8 hours. Then, the volatiles are removed under reduced pressure, and the residual aqueous solution is neutralized with $NaHCO_3$ to pH ~8 and is extracted with nitrobenzene (3 × 75 mL). After removing the solvent, the resulting residue is purified by column chromatography on silica gel (450 g) using $CHCl_3/CH_3OH$ (9:1) as eluent.

1,4-Bis(pyrazol-3(5)-yl)butane. Colorless crystalline solid. Yield: 3.728 g (80%). ^{1}H NMR (400 MHz, $CDCl_3$): δ 7.48 (d, 2H, 3-*H*-pz, *J* = 2 Hz), 6.05 (d, 2H, 4-*H*-pz, *J* = 1.6 Hz), 2.73 (t, 4H, $CH_2(CH_2)_2CH_2$, *J* = 6.2 Hz), 1.78 (quint, 4H, $CH_2CH_2CH_2CH_2$, *J* = 3.3 Hz) ppm. ^{13}C NMR (400 MHz, $CDCl_3$): δ 147.91, 134.61, 103.56, 28.09, 26. 31 ppm. HRMS (ESI-TOF) *m*/*z*: $[M–H]^-$ calcd for $C_{10}H_{13}N_4$ 189.1140; found 189.1149.

1,5-Bis(pyrazol-3(5)-yl)pentane. Colorless viscous oil. Yield: 3.826 g (79%). ^{1}H NMR (400 MHz, $CDCl_3$): δ 7.44 (d, 2H, 3-*H*-pz, *J* = 2 Hz), 6.00 (d, 2H, 4-*H*-pz, *J* = 1.6 Hz), 2.68 (t, 4H, $CH_2(CH_2)_3CH_2$, *J* = 7 Hz), 1.67 (quint, 4H, $CH_2CH_2CH_2CH_2CH_2$, *J* = 7.3 Hz), 1.27 (quint, 2H, $(CH_2)_2CH_2(CH_2)_2$, *J* = 7.6 Hz) ppm. ^{13}C NMR (400 MHz, $CDCl_3$): δ 147.67, 134.40, 103.48, 28.38, 27.29, 26.08 ppm. HRMS (ESI-TOF) *m*/*z*: $[M–H]^-$calcd for $C_{11}H_{15}N_4$ 203.1297; found 203.1301.

General procedure for the synthesis of homoleptic CO_3- and SO_4-nanojars with L2 or L3.

To a solution of $Cu(NO_3)_2{\cdot}2.5H_2O$ (0.1437 g, 0.618 mmol) in THF (15 mL) is added 1,2-bis(pyrazol-3(5)-yl)ethane (H_2**L2**) (0.0500 g, 0.309 mmol) or 1,3-bis(pyrazol-3(5)-yl)propane (H_2**L3**) (0.0544 g, 0.309 mmol), and either Bu_4NOH (55% in H_2O, 0.6039 g, 1.280 mmol) or a solution of Bu_4NHSO_4 (0.2097 g, 0.618 mmol) and Bu_4NOH (55% in H_2O, 0.8747 g, 1.854 mmol) in THF (5 mL). After stirring for 3 days, the deep blue solution is filtered and slowly added into water (150 mL) under vigorous stirring. The blue precipitate is filtered out, washed thoroughly with water, and dried in vacuum. Yield: 0.0722–0.1013 g (~72–99 %).

Alternative synthesis of CO_3-nanojars with H_2L3.

$Cu(NO_3)_2{\cdot}2.5H_2O$ (0.1560 g, 0.670 mmol), 1,3-bis(pyrazol-3(5)-yl)propane (H_2**L3**) (0.0591 g, 0.335 mmol), NaOH (0.0554 g, 1.478 mmol), $Na_2CO_3{\cdot}H_2O$ (0.0832 g, 0.670 mmol), and Bu_4NOH (55% in H_2O, 0.0226 g, 0.048 mmol) are stirred in THF (15 mL) for 3 days. The deep blue solution is filtered and slowly added into water (150 mL) under vigorous stirring. The

blue precipitate is filtered out, washed thoroughly with water, and dried in vacuum. Yield: 0.0959 g (~77%).

Synthesis of $(Bu_4N)_2[CO_3 \subset \{Cu_{26}(OH)_{26}(L3)_{13}\}]$.

$Cu(NO_3)_2 \cdot 2.5H_2O$ (0.0660 g, 0.284 mmol), 1,3-bis(pyrazol-3(5)-yl)propane (H_2**L3**) (0.0500 g, 0.284 mmol) and Bu_4NOH (1 M in H_2O, 0.6380 g, 0.638 mmol) are stirred in THF (10 mL) overnight (~14 h). The deep blue solution is filtered and added slowly into water (100 mL) under vigorous stirring. The blue precipitate is filtered out, washed thoroughly with water, and dried in vacuum. Yield: 0.0514 g (96%).

General procedure for the synthesis of heteroleptic CO_3- and SO_4-nanojars with L4/pz, L5/pz or L6/pz mixtures.

To a solution of $Cu(NO_3)_2 \cdot 2.5H_2O$ (0.1972 g, 0.848 mmol) and 1*H*-pyrazole (0.0289 g, 0.424 mmol) in THF (15 mL) is added either 1,4-bis(pyrazol-3(5)-yl)butane (H_2**L4**; 0.0403 g, 0.212 mmol), 1,5-bis(pyrazol-3(5)-yl)pentane (H_2**L5**; 0.0433 g, 0.212 mmol) or 1,6-bis(pyrazol-3(5)-yl)hexane (H_2**L6**; 0.0464 g, 0.212 mmol), and either Bu_4NOH (55% in H_2O, 0.8286 g, 1.757 mmol) or a mixture of $(Bu_4N)_2SO_4$ (50% in H_2O, 0.0352 g, 0.0300 mmol) and Bu_4NOH (55% in H_2O, 0.8000 g, 1.696 mmol). After stirring for 3 days, the deep blue solution is filtered and slowly added into water (200 mL) under vigorous stirring. The blue precipitate is filtered out, washed thoroughly with water, and dried in vacuum. Yield: 0.1168–0.1823 g.

Synthesis of $Cu_4(OH)_2(L3)_2(NO_3)_2$.

$Cu(NO_3)_2 \cdot 2.5H_2O$ (0.1410 g, 0.60 mmol), 1,3-bis(pyrazol-3(5)-yl)propane (H_2**L3**) (0.0533 g, 0.30 mmol) and NaOH (0.0360 g, 0.90 mmol) are stirred in THF (15 mL) for 3 days. The dark blue solution is filtered, and the solvent is evaporated in vacuum leaving behind a dark blue solid. Yield: 0.1280 g (~97%).

Selectivity experiments (CO_3^{2-} vs. SO_4^{2-}) using homoleptic pyrazole-, L2- or L3-based nanojars.

To a solution of $Cu(NO_3)_2 \cdot 2.5H_2O$ (0.1711 g, 0.736 mmol) in THF (10 mL) is added either 1*H*-pyrazole (0.0501 g, 0.736 mmol), 1,2-bis(pyrazol-3(5)-yl)ethane (H_2**L2**; 0.0595 g, 0.368 mmol) or 1,3-bis(pyrazol-3(5)-yl)propane (H_2**L3**; 0.0648 g, 0.284 mmol). Then, a solution of Bu_4NOH (55% in H_2O, 1.3889 g, 2.944 mmol), Bu_4NHSO_4 (0.2499 g, 0.736 mmol) and Bu_4NHCO_3 (0.2234 g, 0.736 mmol) in THF (10 mL) is added. Bu_4NHCO_3 is freshly prepared by first bubbling excess CO_2 gas (obtained by sublimation of dry ice) for 1 h through a THF

solution of Bu_4NOH (55% in H_2O, 0.3472 g, 0.736 mmol), and then removing the excess CO_2 and THF in vacuum. After stirring for 3 days, the deep blue solution is poured into water (200 mL) under vigorous stirring, THF is evaporated in vacuum and the blue precipitate is filtered out, washed thoroughly with water, and dried in vacuum. Yield: 0.0929–0.1395 g.

Selectivity experiments (CO_3^{2-} vs. SO_4^{2-}) using heteroleptic nanojars based on L4/pz, L5/pz or L6/pz mixtures.

To a solution of $Cu(NO_3)_2{\cdot}2.5H_2O$ (0.1972 g, 0.848 mmol) and 1*H*-pyrazole (0.0289 g, 0.424 mmol) in THF (10 mL) is added either 1,4-bis(pyrazol-3(5)-yl)butane (H_2**L4**; 0.0403 g, 0.212 mmol), 1,5-bis(pyrazol-3(5)-yl)pentane (H_2**L5**; 0.0433 g, 0.212 mmol) or 1,6-bis(pyrazol-3(5)-yl)hexane (H_2**L6**; 0.0464 g, 0.212 mmol). Then, a solution of Bu_4NOH (55% in H_2O, 0.8143 g, 1.726 mmol), $(Bu_4N)_2SO_4$ (50% in H_2O, 0.0352 g, 0.030 mmol), and Bu_4NHCO_3 (0.0092 g, 0.030 mmol) in THF (10 mL) is added. Bu_4NHCO_3 is freshly prepared by first bubbling excess CO_2 gas (obtained by sublimation of dry ice) for 1 h through a THF solution of Bu_4NOH (55% in H_2O, 0.0143 g, 0.030 mmol), and then removing the excess CO_2 and THF in vacuum. After stirring for 3 days, the deep blue solution is poured into water (200 mL) under vigorous stirring, THF is evaporated in vacuum and the blue precipitate is filtered out, washed thoroughly with water, and dried in vacuum. Yield: 0.1074 –0.1403 g.

Mass spectrometry. Mass spectrometric analysis of the nanojars was performed with a Waters Synapt G1 HDMS instrument, using electrospray ionization (ESI). 10^{-4}–10^{-5} M solutions were prepared in CH_3CN or DMF. Samples were infused by a syringe pump at 5 μL/min and nitrogen was supplied as nebulizing gas at 500 L/h. The electrospray capillary voltage was set to –2.5 or +2.5 kV, respectively, with a desolvation temperature of 110 °C or 150 °C. The sampling and extraction cones were maintained at 40 V and 4.0 V, respectively, at 80 °C. The relative amounts of different nanojar species obtained in the selectivity experiments were calculated by summing up the abundances of the isotope peaks observed within the isotopic envelope of each species, which are assumed to have similar ionization efficiencies.

X-Ray crystallography. Single-crystals were obtained either by vapor diffusion of pentane into a solution of H_2**L4** in chloroform, vapor diffusion of pentane into a solution of $(THP)_2$**L4** in ethyl acetate, or layering of heptane over a solution of $(THP)_2$**L5** in ethyl acetate. X-Ray

diffraction data were collected at 150 K from a single-crystal mounted atop a MiTeGen micromesh mount under Fomblin oil with a Bruker AXS D8 Quest diffractometer equipped with a Photon II charge-integrating pixel array detector (CPAD) using graphite-monochromated Mo-K_α (λ = 0.71073 Å) radiation (for $(THP)_2$**L4** and $(THP)_2$**L5**), or a Bruker AXS D8 Quest diffractometer equipped with a Photon III charge-integrating and photon counting pixel array detector (CPAD) using Cu-K_a (λ = 1.54178 Å) monochromated using laterally graded multilayer (Goebel) mirrors (for H_2**L4**). The data were collected using APEX3,[51] integrated using SAINT[52] and scaled and corrected for absorption and other effects using SADABS.[53] The structures were solved by employing direct methods using ShelXS[54] and refined by full-matrix least squares on F^2 using ShelXL.[55] C–H hydrogen atoms were placed in idealized positions and refined using the riding model. The tetrahydropyran moiety in $(THP)_2$**L4** was refined as disordered by a slight rotation. The two disordered moieties were restrained to have similar geometries. U^{ij} components of ADPs for disordered atoms closer to each other than 2.0 Å were restrained to be similar. Subject to these conditions the occupancy ratio refined to 0.585(11)/0.451(11). Crystallographic data are summarized in Table 2.

	H_2L4	**$(THP)_2$L4**	**$(THP)_2$L5**
Formula	$C_{10}H_{14}N_4$	$C_{20}H_{30}N_4O_2$	$C_{21}H_{32}N_4O_2$
FW ($g \cdot mol^{-1}$)	190.25	358.48	372.50

Table 2. Crystallographic data.

Crystal system	Triclinic	Monoclinic	Triclinic
Space group	P ī	$P2_1/c$	P ī
a (Å)	7.5321(3)	16.5743(11)	8.2970(3)
b (Å)	8.0983(3)	4.6460(3)	9.2575(3)
c (Å)	9.2836(4)	12.7547(9)	15.0135(5)
α (deg)	71.4315(18)	90.000	87.5026(18)
β (deg)	73.3773(17)	97.570(3)	80.0574(19)
γ (deg)	66.8118(19)	90.000	64.7954(17)
V (Å^3)	484.97(3)	973.61(11)	1027.14(6)
Z	2	2	2
D_{calc} (g·cm^{-3})	1.303	1.223	1.204
μ (mm^{-1})	0.660	0.081	0.079
θ range (deg)	5.11–78.75	3.30–33.21	2.43–33.28
Reflns collected	4616	21842	21263
R_{int}	0.0293	0.0496	0.0727
Obsd reflns [$I > 2\sigma(I)$]	1780	2575	4424
Data/restraints/parameters	1952/0/133	3653/48/164	7387/0/244
GOF (on F^2)	1.126	1.032	1.035
R factors [$I > 2\ \sigma(I)$]	R_1 = 0.0459 wR_2 = 0.0492	R_1 = 0.0455 wR_2 = 0.0699	R_1 = 0.0491 wR_2 = 0.1287
R factors (all data)	R_1 = 0.1321 wR_2 = 0.1352	R_1 = 0.1177 wR_2 = 0.1316	R_1 = 0.1221 wR_2 = 0.1428
Maximum peak/hole (e·Å^{-3})	0.268/−0.216	0.301/−0.193	0.395/−0.234
CCDC number	2090886	2090887	2090888

Conflicts of interest

There are no conflicts to declare.

Acknowledgements

This material is based on work supported by the National Science Foundation under Grant No. CHE-1808554. Funding for the single-crystal X-ray diffractometer was provided by the National Science Foundation through the Major Research Instrumentation Program under Grant No. CHE-1625543.

References

[1] E. Aguilar-Barajas, C. Díaz-Pérez, M. I. Ramírez-Díaz, H. Riveros-Rosas and C. Cervantes, *Biometals*, 2011, **24**, 687–707.

[2] L. N. Pincus, H. E. Rudel, P. V. Petrović, S. Gupta, P. Westerhoff, C. L. Muhich and J. B. Zimmerman, *Environ. Sci. Technol.*, 2020, **54**, 9769–9790.

[3] B. L. Jacobson and F. A. Quiocho, *J. Mol. Biol.*, 1988, **204**, 783–787.

[4] M. Elias, A. Wellner, K. Goldin-Azulay, E. Chabriere, J. A. Vorholt, T. J. Erb and D. S. Tawfik, *Nature*, 2012, **491**, 134–137.

[5] D. Gonzalez, M. Richez, C. Bergonzi, E. Chabriere and M. Elias, *Sci. Rep.*, 2014, **4**, 6636.

[6] P. Chakrabarti, *J. Mol. Biol.*, 1993, **234**, 463–482.

[7] T. T. Waldron, M. A. Modestou and K. P. Murphy, *Protein Sci.*, 2003, **12**, 871–874.

[8] (*a*) B. A. Moyer and R. P. Singh (eds.), *Fundamentals and Applications of Anion Separations*. Kluwer, New York **2004**. (*b*) K. Bowman-James, A. Bianchi and E. García-España, (eds.), *Anion Coordination Chemistry*. Wiley-VCH, Weinheim **2012**. (*c*) J. L. Sessler, P. A. Gale and W.-S. Cho, *Anion Receptor Chemistry* (Monographs in Supramolecular Chemistry), The Royal Society of Chemistry **2006**. (*d*) A. Bianchi, K. Bowman-James and E. García-España (eds.), *Supramolecular Chemistry of Anions*. Wiley-VCH **1997**.

[9] (*a*) E. A. Katayev, P. J. Melfi and J. L. Sessler, "Anion-Binding Macrocycles", in *Modern Supramolecular Chemistry: Strategies for Macrocycle Synthesis*, F. Diederich, P. J. Stang and R. R. Tykwinski (eds.), Wiley-VCH, Weinheim **2008**, pp. 315–347. (*b*) J. W. Steed and J. L. Atwood, "Binding of Anions", Chapter 4 in *Supramolecular Chemistry*, John Wiley & Sons **2009**, pp. 223–284. (*c*) R. S. Dickins and D. Parker, "Signalling Reversible Anion Binding in Aqueous Media", in *Macrocyclic Chemistry: Current Trends and Future Perspectives*, K. Gloe (ed.), Springer **2005**, pp. 121–136. (*d*) B. D. Smith, "Ion-Pair Recognition by Ditopic Macrocyclic Receptors", in *Macrocyclic Chemistry: Current Trends and Future Perspectives*, K. Gloe (ed.), Springer **2005**, pp. 137–151. (*e*) S. J. Brooks and P. A. Gale, "Cyclic and Acyclic Amidopyrrole Containing Anion Receptors", in *Macrocyclic Chemistry: Current Trends and Future Perspectives*, K. Gloe (ed.), Springer **2005**, pp. 153–172. (*f*) Md. A. Hossain, S. O. Kang and K. Bowman-James, "Structural Aspects of Halides with Cryptands", in *Macrocyclic Chemistry: Current Trends and Future Perspectives*, K. Gloe (ed.), Springer **2005**, pp. 173–188. (*g*) J. Nelson, V. McKee and R. M. Town, "Oxoanion Selectivity with Protonated Azacryptand Hosts: The Influence of Hydration on Structure and Stability", in *Macrocyclic Chemistry: Current Trends and Future Perspectives*, K. Gloe (ed.), Springer **2005**, pp. 189–201. (*h*) *Supramolecular Chemistry: From Molecules to Nanomaterials*, Vol. 3: Molecular Recognition, J. W. Steed and P. A. Gale (eds.), Wiley **2012**, pp. 731–1380. (*i*) J. R. Dobscha, Y. Liu and A. H. Flood, "Shape-Persistent Anion Receptors", in *Comprehensive Supramolecular Chemistry II*; Elsevier **2016**, pp. 329–348**.** (*j*) S. Kubik and D. Mungalpara, "Amino Acid-Based Receptors", in *Comprehensive Supramolecular Chemistry II*; Elsevier **2016**, pp. 293–310. (*k*) M. S. Taylor, "Halogen Bond-Based Receptors", in *Comprehensive Supramolecular Chemistry II*; Elsevier **2016**, pp. 401–416.

[10] (*a*) P. A. Gale and W. Dehaen (eds.), "Anion Recognition in Supramolecular Chemistry", *Top. Heterocycl. Chem.,* 2010, **24**, 1–366. (*b*) Themed issue: "Supramolecular chemistry of anionic species", P. A. Gale and T. Gunnalaugsson (eds.), *Chem. Soc. Rev.,* 2010, **39**, 3597–4003. (*c*) Themed issue: "35 Years of Synthetic Anion Receptor Chemistry 1968–2003", P. A. Gale (ed.), *Coord. Chem. Rev.,* 2003, **240**, 1–226. (*d*) Themed issue: "Anion Coordination Chemistry", P. A. Gale (ed.), *Coord. Chem. Rev.,* 2006, **250**, 2917–3244.

[11] (*a*) I. Ravikumar and P. Ghosh, *Chem. Soc. Rev.,* 2012, **41**, 3077–3098. (*b*) S. Fukuzumi, K. Ohkubo, F. D'Souza and J. L. Sessler, *Chem. Commun.,* 2012, **48**, 9801–9815. (*c*) M. Arunachalam and P. Ghosh, *Chem. Commun.,* 2011, **47**, 8477–8492. (*d*) K. M. Mullen and P. D. Beer, *Chem. Soc. Rev.,* 2009, **38**, 1701–1713. (*e*) S. Kubik, *Chem. Soc. Rev.,* 2009, **38**, 585–605. (*f*) E. A. Katayev, Y. A. Ustynyuk and J. A. Sessler, *Coord. Chem. Rev.,* 2006, **250**, 3004–3037. (*g*) K. Bowman-James, *Acc. Chem. Res.,* 2005, **38**, 671–678. (*h*) V. McKee, J. Nelson and R. M. Town, *Chem. Soc. Rev.,* 2003, **32**, 309–325. (*i*) R. Custelcean, *Top. Curr. Chem.* 2012, **322**, 193–216. (*j*) P. A. Gale, E. N. W. Howe and X. Wu, *Chem,* 2016, **1**, 351–422. (*k*) A. H. Flood, *Beilstein J. Org. Chem*., 2016, **12**, 611–627. (*l*) R. Dutta and P. Ghosh, *Chem. Commun*., 2015, **51**, 9070–9084. (*m*) R. B. P. Elmes and K. A. Jolliffe, *Chem. Commun.,* 2015, **51**, 4951–4968. (*n*) M. J. Langton, C. J. Serpell and P. D. Beer, *Angew. Chem. Int. Ed*., 2016, **55**, 1974–1987. (*o*) G. Alibrandi,

V. Amendola, G. Bergamaschi, L. Fabbrizzi and M. Licchelli, *Org. Biomol. Chem*., 2015, **13**, 3510–3524. (*p*) R. Dutta and P. Ghosh, *Chem. Commun.,* 2014, **50**, 10538–10554. (*r*) R. Custelcean, *Chem. Commun.,* 2013, **49**, 2173–2182. (*s*) P. A. Gale and C. Caltagirone, *Chem. Soc. Rev.,* 2015, **44**, 4212–4227. (*t*) A. Caballero, F. Zapata and P. D. Beer, *Coord. Chem. Rev*., 2013, **257**, 2434–2455. (*u*) J. Cai and J. L. Sessler, *Chem. Soc. Rev*., 2014, **43**, 6198–6213. (*w*) P. Molina, F. Zapata and A. Caballero, *Chem. Rev.*, 2017, **117**, 9907–9972. (*x*) L. Chen, S. N. Berry, X. Wu, E. N. W. Howe and P. A. Gale, *Chem*, 2020, **6**, 61–141. (*y*) S. A. Boer, E. M. Foyle, C. M. Thomas and N. G. White, *Chem. Soc. Rev.,* 2019, **48**, 2596–2614.

[2] (*a*) K. P. McDonald, Y. Hua, S. Lee and A. H. Flood, *Chem. Commun.,* 2012, **48**, 5065–5075. (*b*) B. M. Rambo and J. L. Sessler, *Chem. Eur. J.,* 2011, **17**, 4946–4959. (*c*) A. D. Hamilton and K. Choi, *Coord. Chem. Rev.,* 2003, **240**, 101–110.

[3] S. O. Kang, J. M. Llinares, V. W. Day and K. Bowman-James, *Chem. Soc. Rev.,* 2010, **39**, 3980–4003.

[4] P. Ballester, *Chem. Soc. Rev.,* 2010, **39**, 3810–3830.

[5] (a) S. Kubik, *Acc. Chem. Res*., 2017, **50**, 2870–2878. (b) J. Bartl and S. Kubik, *ChemPlusChem*, 2020, **85**, 963–969.

[6] (*a*) A. Caballero, F. Zapata, N. G. White, P. J. Costa, V. Félix and P. D. Beer, *Angew. Chem. Int. Ed.,* 2012, **51**, 1876–1880. (*b*) L. M. Hancock, E. Marchi, P. Ceroni and P. D. Beer, *Chem. Eur. J.,* 2012, **18**, 11277–11283. (*c*) N. H. Evans, C. J. Serpell and P. D. Beer, *Chem. Commun.,* 2011, **47**, 8775–8777. (*d*) A. Brown, K. M. Mullen, J. Ryu, M. J. Chmielewski, S. M. Santos, V. Felix, A. L. Thompson, J. E. Warren, S. I. Pascu and P. D. Beer, *J. Am. Chem. Soc.,* 2009, **131**, 4937–4952. (*e*) J. Y. C. Lim, I. Marques, A. L. Thompson, K. E. Christensen, V. Félix and P. D. Beer, *J. Am. Chem. Soc*., 2017, **139**, 3122–3133.

[7] (*a*) R. Custelcean, J. Bosano, P. V. Bonnesen, V. Kertesz and B. P. Hay, *Angew. Chem. Int. Ed*., 2009, **48**, 4025–4029. (*b*) D. J. Mercer and S. J. Loeb, *Chem. Soc. Rev.,* 2010, **39**, 3612–3620. (*c*) T. Zhang, L.-P. Zhou, X.-Q. Guo, L.-X. Cai and Q.-F. Sun, *Nat. Commun*., 2017, **8**, 15898.

[8] (*a*) R. Custelcean and B. A. Moyer, *Eur. J. Inorg. Chem.,* 2007, 1321–1340. (*b*) R. Custelcean, *Chem. Soc. Rev.,* 2010, **39**, 3675–3685. (*c*) X. Wu, L. K. Macreadie and P. A. Gale, *Coord. Chem. Rev.*, 2021, **432**, 213708.

[9] (*a*) E. Delgado-Pinar, C. Rotger, A. Costa, M. N. Piña, H. R. Jiménez, J. Alarcón and E. García-España, *Chem. Commun.,* 2012, **48**, 2609–2611. (*b*) J. Zhang, X. Xu, C. Yang, F. Yang and Y. Yang, *Anal. Chem*., 2011, **83**, 3911–3917. (*c*) D. P. Cormode, J. J. Davis and P. D. Beer, *J. Inorg. Organomet. Polym*., *2008*, **18**, 32–40. (*d*) P. D. Beer, D. P. Cormode and J. J. Davis, *Chem. Commun*., 2004, 414–415. (*e*) P. Sokkalingam, S.-J. Hong, A. Aydogan, J.-L. Sessler and C.-H. Lee, *Chem. Eur. J.,* 2013, **19**, 5860–5867.

[20] (*a*) S. Valiyaveettil, J. F. J. Engbersen, W. Verboom and D. N. Reinhoudt, *Angew. Chem. Int. Ed.,* 1993, **32**, 900–901. (*b*) M. M. G. Antonisse and D. N. Reinhoudt, *Chem. Commun.,* 1998, 443–448.

[21] P. Bose, I. Ravikumar and P. Ghosh, *Inorg. Chem.,* 2011, **50**, 10693–10702.

[22] (*a*) S. K. Dey, B. K. Datta and G. Das, *CrystEngComm,* 2012, **14**, 5305–5314. (*b*) S. K. Dey and G. Das, *Chem. Commun.,* 2011, **47**, 4983–4985. (*c*) S. K. Dey and G. Das, *Cryst. Growth Des.,* 2011, **11**, 4463–4473.

[23] (*a*) S. K. Dey, B. Ojha and G. Das, *CrystEngComm,* 2011, **13**, 269–278. (*b*) S. K. Dey, A. Pramanik and G. Das, *CrystEngComm,* 2011, **13**, 1664–1675.

[24] (*a*) B. Akhuli, I. Ravikumarb and P. Ghosh, *Chem. Sci.,* 2012, **3**, 1522–1530. (*b*) S. K. Dey, R. Chutia and G. Das, *Inorg. Chem.,* 2012, **51**, 1727–1738. (*c*) R. Rajbanshi, B. A. Moyer and R. Custelcean, *Cryst. Growth Des.,* 2011, **11**, 2702–2706. (d) C. Jia, B. Wu, S. Li, X. Huang, Q. Zhao, Q.-S. Li and X.-J. Yang, *Angew. Chem. Int. Ed*., 2011, **50**, 486–490. (e) U. Manna and G. Das, *New J. Chem.,* 2018, **42**,

19164–19177. (*f*) S. Kumar Dey, Archana, S Pereira, S S. Harmalkar, S. N. Mhaldar, V. V. Gobrea and C. Janiak, *CrystEngComm*, 2020, **22**, 6152–6160.
[25] (*a*) S. K. Dey and G. Das, *Dalton Trans.,* 2012, **41**, 8960–8972. (*b*) P. G. Young and K. A. Jolliffe, *Org. Biomol. Chem*., 2012, **10**, 2664–2672. (*c*) A. Basu and G. Das, *Dalton Trans*., 2012, **41**, 10792–10802. (*d*) N. Busschaert, M. Wenzel, M. E. Light, P. Iglesias-Hernandez, R. Perez-Tomas and P. A. Gale, *J. Am. Chem. Soc*., 2011, **133**, 14136–14148. (*e*) S. K. Dey and G. Das, *Dalton Trans*., 2011, **40**, 12048–12051. (*f*) M. Emami Khansari, A. Mirchi, A. Pramanik, C. R. Johnson, J. Leszczynski and Md. A. Hossain, *Sci. Rep.*, 2017, ***7***, 6032.
[26] (*a*) S. Li, C. Jia, B. Wu, Q. Luo, X. Huang, Z. Yang, Q.-S. Li and X.-Y. Yang, *Angew. Chem. Int. Ed.,* 2011, **50**, 5721–5724. (*b*) C. Jia, B. Wu, S. Li, Z. Yang, Q. Zhao, J. Liang, Q.-S. Li and X.-Y. Yang, *Chem. Commun.,* 2010, **46**, 5376–5378. (*c*) C. Jia, B. Wu, S. Li, X. Huang and X.-J. Yang, *Org. Lett*., 2010, **12**, 5612–5615. (*d*) C. Caltagirone, J. R. Hiscock, M. B. Hursthouse, M. E. Light and P. A. Gale, *Chem. Eur. J.,* 2008, **14**, 10236–10243. (*e*) V. Blažek Bregović, N. Basarić and K. Mlinarić-Majerski, Coord. *Chem. Rev*., 2015, **295**, 80–124
[27] (*a*) R. Custelcean, P. V. Bonnesen, N. C. Duncan, X. Zhang, L. A. Watson, G. Van Berkel, W. B. Parson and B. P. Hay, *J. Am. Chem. Soc.,* 2012, **134**, 8525–8534. (*b*) R. Custelcean, P. V. Bonnesen, B. D. Roach and N. C. Duncan, *Chem. Commun.,* 2012, **48**, 7438–7440. (*c*) C. R. Bondy, P. A. Gale and S. J. Loeb, *J. Am. Chem. Soc.,* 2004, **126**, 5030–5031.
[28] (*a*) Y. Li and A. H. Flood, *Angew. Chem. Int. Ed.,* 2008, **47**, 2649–2652. (*b*) Y. Li and A. H. Flood, *J. Am. Chem. Soc.,* 2008, **130**, 12111–12122. (*c*) Y. Liu, A. Sengupta, K. Raghavachari and A. H. Flood, *Chem*, 2017, **3**, 411–427. (*d*) Y. Liu, W. Zhao, C.-H. Chen and A. H. Flood, *Science*, 2019, **365**, 159–161.
[29] (*a*) B. A. Moyer, L. H. Delmau, C. J. Fowler, A. Ruas, D. A. Bostick, J. L. Sessler, E. Katayev, G. D. Pantos, J. M. Llinares, M. A. Hossain, S. O. Kang and K. Bowman-James, *Adv. Inorg. Chem.,* 2006, **59**, 175–204. (*b*) B. A. Moyer, R. Custelcean, B. P. Hay, J. L. Sessler, K. Bowman-James, V. W. Day and S.-O. Kang, *Inorg. Chem*., 2013, **52**, 3473–3490.
[30] M. S. H. Bader, *J. Pet. Sci. Eng.,* 2007, **55**, 93–110.
[3] H. Zhou, Y. Zhao, G. Gao, S. Li, J. Lan and J. You, *J. Am. Chem. Soc.*, 2013, **135**, 14908–14911.
[32] Y. Marcus, *Ions in Water and Biophysical Implications: From Chaos to Cosmos*; Springer: Dordrecht, The Netherlands, **2012**, page 66.
[33] N. J. Williams, C. A. Seipp, K. A. Garrabrant, R. Custelcean, E. Holguin, J. K. Keum, R. J. Ellis and B. A. Moyer, *Chem. Commun.*, 2018, **54**, 10048–10051.
[34] G. Mezei, Selective Extraction of Anions from Solutions. U.S. Patent 9,901,901 B2, 27 February 2018; U.S. Patent 10,087,197 B2, 2 October 2018; European Patent 2852558 B1, 9 September 2020.
[35] I. R. Fernando, S. A. Surmann, A. A. Urech, A. M. Poulsen and G. Mezei, *Chem. Commun.,* 2012, **48**, 6860–6862.
[36] G. Mezei, *Chem. Commun*., 2015, **51**, 10341–10344.
[37] B. M. Ahmed, B. R. Szymczyna, S. Jianrattanasawat, S. A. Surmann and G. Mezei, *Chem. Eur. J.,* 2016, **22**, 5499–5503.
[38] B. M. Ahmed, B. Calco and G. Mezei, *Dalton Trans*., 2016, **45**, 8327–8339.
[39] B. M. Ahmed, C. K. Hartman and G. Mezei, *Inorg. Chem.,* 2016, **55**, 10666–10679.
[40] B. M. Ahmed and G. Mezei, *Inorg. Chem*., 2016, **55**, 7717–7728.
[4] C. K. Hartman and G. Mezei, *Inorg. Chem.,* 2017, **56**, 10609–10624.
[42] V. W. Liyana Gunawardana and G. Mezei, *New J. Chem.,* 2018, **42**, 17195–17202.
[43] A. Eiberweiser, A. Nazet, G. Hefter and R. Buchner, *J. Phys. Chem. B,* 2015, **119**, 5270–5281.
[44] J. Bergman and L. Venemalm, *J. Org. Chem.*, 1992, **57**, 2495–2497.

[45] T. B. Poynder, D. P. Savaliya, A. Molino, D. J. D. Wilson and J. L. Dutton, *Aust. J. Chem.*, 2019, **72**, 614–619.
[46] B. B. Wang and P. J. Smith, *Tetrahedron Lett.*, 2003, **44**, 8967–8969.
[47] B. M. Ahmed and G. Mezei, *Chem. Commun.,* 2017, **53**, 1029–1032.
[48] G. Mezei, P. Baran and R. G. Raptis, *Angew. Chem. Int. Ed.,* 2004, **43**, 574–577.
[49] R. Doi, M. Shibuya, T. Murayama, Y. Yamamoto and Y. Iwabuchi, *J. Org. Chem.*, 2015, **80**, 401–413.
[50] B. M. Ahmed and G. Mezei, *RSC Adv.*, 2015, **5**, 24081–24093.
[5] Bruker APEX3. Bruker AXS Inc., Madison, Wisconsin, USA, 2016.
[52] Bruker SAINT v.8.38A. Bruker AXS Inc., Madison, Wisconsin, USA, 2017.
[53] Krause, L.; Herbst-Irmer, R.; Sheldrick, G. M.; Stalke, D. *J. Appl. Cryst.*, 2015, **48**, 3–10.
[54] Sheldrick, G. M. *Acta Cryst.*, 2008, **A64**, 112–122.
[55] Sheldrick, G. M. *Acta Cryst.*, 2015, **C71**, 3–8.